Nanoscale Advances

ROYAL SOCIETY OF CHEMISTRY

PAPER

View Article Online
View Journal | View Issue

Cite this: *Nanoscale Adv.*, 2021, **3**, 6669

Metal–organic framework combined with CaO_2 nanoparticles for enhanced and targeted photodynamic therapy†

Xinran Sun, Kaixiu Chen, Yingyan Liu, Guoda Zhang, Min Shi, Pengfei Shi* and Shusheng Zhang *

Received 6th August 2021
Accepted 4th September 2021

DOI: 10.1039/d1na00610j

rsc.li/nanoscale-advances

Photodynamic therapy (PDT) has been rapidly developed as an effective therapeutic approach in clinical settings. However, hypoxia seriously limits the effectiveness of PDT. Here, we report a porphyrin-based metal–organic framework combined with hyaluronate-modified CaO_2 nanoparticles (PCN-224-CaO_2-HA) to target and enhance PDT efficacy. CaO_2 reacts with H_2O or weak acid to produce O_2, overcoming the hypoxia problem. Hyaluronate protects CaO_2 and specifically targets the CD44 receptor, which is highly expressed on tumor cell membranes, performing targeted therapy. After PDT treatment *in vitro*, the survival rates of 4T1 and MCF-7 tumor cells were 14.58% and 22.45%, respectively. The fluorescence imaging showed that PCN-224-CaO_2-HA effectively aggregated in the tumor after 12 h of its intravenous injection into tumor-bearing mice. PCN-224-CaO_2-HA exhibited efficacious tumor growth inhibition *via* enhanced PDT. Overall, this nanosystem providing *in situ* oxygen production was successfully used for targeted PDT with a significantly enhanced therapeutic efficacy *in vitro* and *in vivo*.

Introduction

To overcome the threat of cancer to human health, photodynamic therapy (PDT) is a rapidly developing effective therapeutic approach that can be used against minimally invasive tumors.[1–3] PDT treatment is based on the administration of a photosensitizer (PS) that is able to accumulate in tumors, followed by local irradiation of the tumor with a light of a specific wavelength to activate the PS, which in turn stimulates oxygen (O_2) to generate reactive oxygen species (ROS), particularly singlet oxygen ($^1O_2$), which destroys cancer cells.[4–6] By localizing the PS and light, PDT can selectively cause tumor cells apoptosis and necrosis without damaging surrounding normal tissues.[7] As a result, PDT has been used to treat mesothelioma, pancreatic cancer, and head and neck cancer in clinical settings.[8–10] As the investigation on PDT treatment has progressed, most of the attention in recent years has focused on how to improve photodynamic efficiency.[11–13] According to the three fundamental conditions of PDT, research has been devoted to PS design and synthesis,[14] enhancing their ability to absorb light wavelength[15] and enhancing the production of O_2.[16] Since the first PS hematoporphyrin was used in the early 1980s, a series of porphyrin derivatives, including chlorins, phthalocyanines, and naphthalocyanines, have been explored.[17] However, the low uptake into the tumor, relative poor tissue penetration, suboptimal tumor accumulation and poor aqueous solubility or dispersity limit their use as a therapeutic approach in clinical practice.[18] The advent of nanotechnology promoted a new generation of PS, which is carried by nanomaterials to improve its accumulation into the tumor and eliminate organic hydrotropes.[19] In 2014, nanoscale metal–organic frameworks (nMOFs) were constructed with a PS as the ligand, providing a new strategy for PDT.[20] The regular arrangement of PS in nMOFs avoids the self-quenching of PS, and the porosity of nMOFs facilitates the diffusion of $^1O_2$. Furthermore, nMOFs present good biocompatibility and biodegradability, making them most promising PS, predicted to become the fourth generation of PS.[21,22]

The localization of O_2 molecules in tissues is an essential aspect for effective PDT. However, the uncontrollable growth of tumor cells, as well as the dysregulated formation of blood vessels in the tumor, inevitably leads to cancer hypoxia, which is a common phenomenon in tumors, which seriously restricts PDT efficiency.[23] Recently, a large number of nMOFs with catalytic activity or self-generating ability to produce ROS have been applied in PDT. A $MnFe_2O_4$@MOF nanostructure was used to catalyze H_2O_2 for persistent O_2 production and self-sufficiency.[24] A MOF integrating Pt nanozymes was used to catalyze H_2O_2 to achieve enhanced PDT.[25] A MOF loaded with glucose oxidase and catalase was also used to promote the catalysis of H_2O_2 and produce O_2.[26] But, most of the O_2 generation ability based on

Shandong Provincial Key Laboratory of Detection Technology for Tumor Markers, School of Chemistry and Chemical Engineering, Linyi University, Linyi 276000, Shandong, P. R. China. E-mail: shipengfei913@163.com; shushzhang@126.com

† Electronic supplementary information (ESI) available: DLS, EDS, TEM, UV-vis, FT-IR, PXRD, DCFH fluorescence, CLSM, tumor weight and H & E stained images are listed in ESI. See DOI: 10.1039/d1na00610j

a catalyst might be limited by the specified intracellular concentration of H_2O_2.[27] More recently, CaO_2 was utilized as an O_2 production material in tumor therapy due to its high biocompatibility and efficient O_2-evolving ability.[28–32] Nevertheless, the aqueous instability of CaO_2 prompts that a protectant is essential to avoid premature decomposition. Additionally, targeted therapy is crucial to minimize the damage to healthy tissue and enhance the curative effect.[33,34] Although PDT can selectively induce tumor cell apoptosis *via* immobilization with a laser, the accumulation of the nanosystem in the tumor is slow and not completely effective in the tumor bed due to the leaky nature of the tumor vasculature.[35] To overcome these limitations, targeting ligands such as small molecules,[36,37] antibodies[38] and aptamers[39] have been conjugated with the nanoparticles. Targeting ligands functionalized with nanoparticles can bind to the cell-surface receptors and enter the cells by receptor-mediated endocytosis, thus enhancing their uptake by cancer cells to achieve targeted therapy.[40]

In this work, an *in situ* oxygen production system was constructed using a porphyrin-based MOF (PCN-224) combined with hyaluronate (HA)-modified CaO_2 nanoparticles, which was used to target and enhance PDT. As shown in Scheme 1, PCN-224 nanoparticles were synthesized firstly. Then, HA-modified CaO_2 nanoparticles were decorated on PCN-224 *in situ* to obtain PCN-224-CaO_2-HA. PCN-224-CaO_2-HA slowly reacted with H_2O or weak acid to produce O_2 in sufficient quantities, solving the hypoxia problem and enhancing the efficacy of PDT. In addition, HA protects the CaO_2 and specifically targets the CD44 receptor, which is highly expressed on the tumor cell membranes of 4T1 and MCF-7 cells, realizing targeted therapy. The experimental results indicate that PCN-224-CaO_2-HA enhances the therapeutic effect and the targeting efficiency of PDT *in vitro* and *in vivo*.

Results and discussion

Firstly, PCN-224 nanoparticles were synthesized according to our previous work when heating $ZrOCl_2$ and H_2TCPP in *N*,*N*′-dimethylformamide (DMF) at 90 °C for 5 h.[41] The PCN-224-CaO_2-HA nanoparticles were then obtained by growing HA-modified CaO_2 on the surface of PCN-224 at room temperature. PCN-224 combined with HA-modified CaO_2 was realized by the coordination interactions between HA and Zr^{4+} ions.[42] The morphologies of the obtained PCN-224 and PCN-224-CaO_2-HA were observed by transmission electron microscopy (TEM). Fig. 1a and b show that PCN-224 was characterized with a good monodispersed size distribution of approximately 200 nm. After combination with HA-modified CaO_2, the diameter of PCN-224 and its morphology was almost unchanged. The particle size and dispersivity of PCN-224 and PCN-224-CaO_2-HA were also measured by dynamic light scattering (DLS), as shown in Fig. S1.† Relatively narrow size distributions were observed with diameters of 220 nm (PCN-224) and 245 nm (PCN-224-CaO_2-HA) from the DLS tests. The CaO_2 nanoparticles were found to be

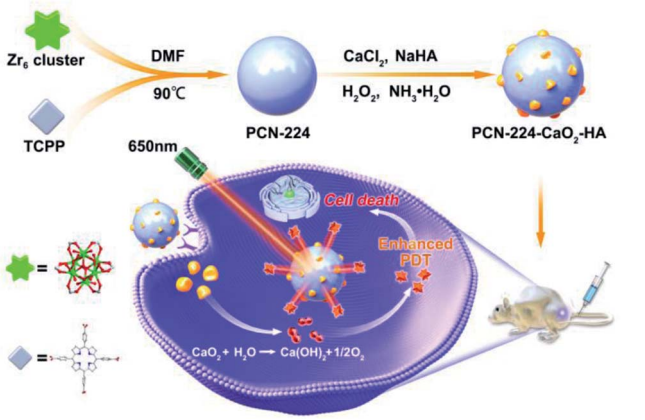

Scheme 1 Schematic representation of PCN-224 combined with hyaluronate (HA)-modified CaO_2 nanoparticles for enhanced photodynamic therapy.

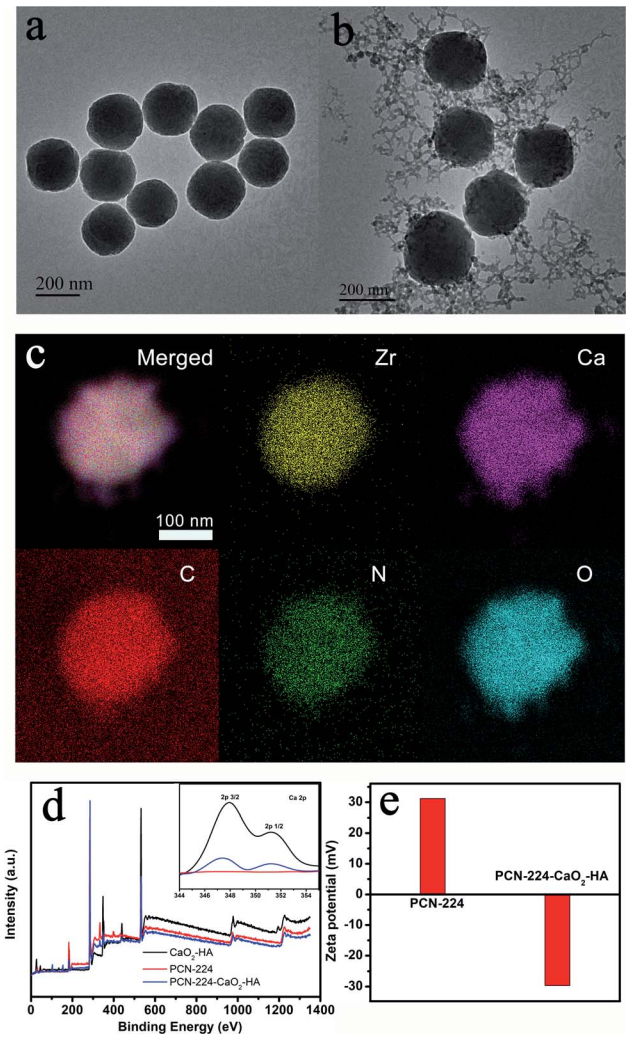

Fig. 1 Characterization of PCN-224 and PCN-224-CaO_2-HA. TEM images of (a) PCN-224 and (b) PCN-224-CaO_2-HA. (c) Elemental mapping of Zr, Ca, C, N and O in PCN-224-CaO_2-HA. (d) XPS spectra of CaO_2-HA, PCN-224 and PCN-224-CaO_2-HA. The inset shows the high-resolution XPS spectrum of Ca 2p. (e) Zeta potential of PCN-224 and PCN-224-CaO_2-HA.

obviously attached to the surface of PCN-224. TEM elemental mapping (Fig. 1c) and energy dispersive spectra (Fig. S2†) showed the homogeneous distribution of Zr, Ca, C, N and O elements in the same particle. Fig. 1d shows the X-ray photoelectron spectroscopy (XPS) of PCN-224-CaO_2-HA, which was performed to determine the elements and the valence state. The binding energies of the elements Zr and Ca were 182.9 eV and 347.9, and 351.2 eV, respectively.

Due to the carboxyl groups in TCPP and hyaluronate, the lower valence state of O (O_2^{2-}) in XPS is indistinguishable. However, the O_2 generation of PCN-224-CaO_2-HA verifies the existence of CaO_2, which was measured using a dissolved oxygen instrument. As shown in Fig. S3,† the dissolved O_2 content of CaO_2 and PCN-224-CaO_2-HA dispersed in water were higher than that of PCN-224. In addition, the zeta potential of PCN-224 changed from 31.2 mV to −29.7 mV after the addition of HA-modified CaO_2 (Fig. 1e). The negative zeta potential originated from the hyaluronate, which suggested that PCN-224 was successfully modified with HA-modified CaO_2. Additionally, pure HA-CaO_2 nanoparticles were prepared in the absence of PCN-224. The as-prepared HA-CaO_2 (Fig. S4†) showed a similar morphology to that of PCN-224-CaO_2-HA. The Fourier-transform infrared (FT-IR) spectra of HA-CaO_2 clearly display the characteristic peak of a carboxyl group, as shown in Fig. S5.† The powder X-ray diffraction (PXRD) patterns of PCN-224 and PCN-224-CaO_2-HA are identical to the simulated one obtained from the single-crystal data of PCN-224, confirming the stability of PCN-224-CaO_2-HA (Fig. S6†). The typical diffraction peaks of CaO_2 in the patterns of PCN-224-CaO_2-HA are not clear, which might be due to the low crystallinity of CaO_2.[16]

TCPP belongs to the porphyrin family, thus making it a highly effective PS for PDT. Therefore, the photophysical properties of PCN-224 and PCN-224-CaO_2-HA were studied in detail. As shown in Fig. 2a, TCPP shows a strong characteristic absorption peak at 419 nm for the Soret band and four peaks at 514, 549, 590 and 645 nm for the Q band. In comparison, PCN-224 and PCN-224-CaO_2-HA show slight red shifts for all the bands relative to TCPP, with peaks at 425, 523, 562, 598, and 653 nm. This redshifting was attributed to the enlarged conjugated area of the porphyrin after the formation of PCN-224, which is in accordance with the reported literature.[43] Importantly, CaO_2 and HA had no effect on the UV-vis absorption of PCN-224. The degradation degree of PCN-224 and PCN-224-CaO_2-HA in phosphate-buffered saline (PBS) and serum were also evaluated by measuring the UV-vis absorption of the released TCPP ligand in the supernatant (Fig. S7 and S8†). As shown in Fig. 2b, PCN-224 and PCN-224-CaO_2-HA were stable in serum. However, PCN-224 was not stable in PBS, and the TCPP ligands were rapidly released in both 5 mM and 10 mM PBS due to the high affinity of Zr^{4+} towards the phosphate ions. In contrast, the stability of the nanocomposite in PBS was greatly improved due to the protection of HA-modified CaO_2. Therefore, the use of PCN-224-CaO_2-HA could be considered in the biomedical field when the phosphate concentration in the blood is less than 5 mM.

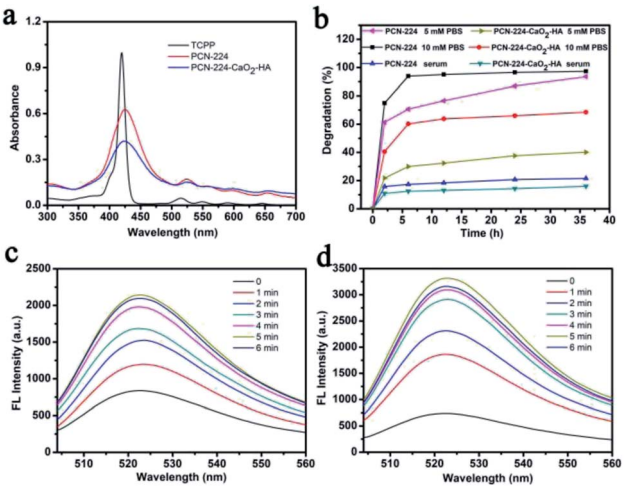

Fig. 2 (a) UV-vis absorption spectra of TCPP, PCN-224 and PCN-224-CaO_2-HA. (b) Degradation rates of PCN-224 and PCN-224-CaO_2-HA under different conditions (5 mM PBS, 10 mM PBS and serum). Fluorescence spectra of DCFH incubated with (c) PCN-224 or (d) PCN-224-CaO_2-HA for different irradiation times.

Next, the ROS generation ability of PCN-224 and PCN-224-CaO_2-HA was monitored using fluorescent 2′,7′-dichlorofluorescein (DCFH) as a probe. Strong fluorescence was observed for CaO_2-HA, PCN-224, and especially for PCN-224-CaO_2-HA, under LED irradiation, indicating excellent ROS production ability of PCN-224-CaO_2-HA, as shown in Fig. S9.† The fluorescence intensity of DCFH increased significantly with increasing LED irradiation time, which corresponded to increased ROS generation efficiency (Fig. 2c and d). Obviously, the ROS generation ability of PCN-224-CaO_2-HA was better than that of PCN-224 in the same LED irradiation time, which confirmed the significant role of CaO_2 in PDT. In addition, to optimize the PDT performance of PCN-224-CaO_2-HA, the ROS capacity of PCN-224 combined with different amounts of CaO_2 was measured. An optimal 3 : 1 ratio of (Zr^{4+}/Ca^{2+}) in PCN-224-CaO_2-HA, measured by inductively coupled plasma (ICP), was able to generate the optimal ROS amount. Meanwhile, the UV-vis absorption spectra of PCN-224-CaO_2-HA still show clear Soret bands and four Q bands when PCN-224 is combined with different amounts of CaO_2 (Fig. S10†).

The cytotoxicity of PCN-224-CaO_2-HA was evaluated using a standard Cell Counting Kit-8 (CCK-8) to assess its biocompatibility. The mouse breast cancer cell line 4T1, human breast cancer cell line MCF-7 and normal human hepatocytes cell line LO2 were incubated with PCN-224-CaO_2-HA at different TCPP gradient concentrations (0, 5, 10, 15, 20, 25 μg mL^{-1}) for 24 h. As shown in Fig. 3a, when the TCPP concentration reached 25 μg mL^{-1}, the survival rate of the 4T1, MCF-7 and LO2 cells still remained above 80%. The cytotoxicity was negligible at concentrations below 20 μg mL^{-1}, which demonstrated that PCN-224-CaO_2-HA exhibits good biocompatibility *in vitro*. In the presence of LED irradiation, the cytotoxicity of PCN-224-CaO_2-HA or PCN-224 towards the 4T1, MCF-7 and LO2 cells was assessed. As shown in Fig. 3b, PCN-224 exerted high phototoxicity towards both cancer and normal cells. CaO_2 reacted with H_2O or weak acid to produce O_2. And HA specifically targeted

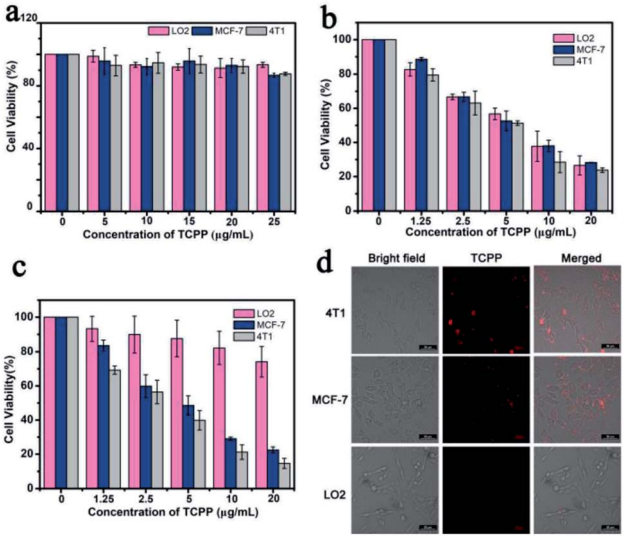

Fig. 3 (a) Cytotoxicity studies by CCK-8 assay for 4T1, MCF-7 and LO2 cells after incubation with various concentrations of PCN-224-CaO_2-HA for 24 h. Cell viability after incubation with (b) PCN-224 or (c) PCN-224-CaO_2-HA under LED irradiation for 10 min. (d) Confocal fluorescence images of cells incubated with PCN-224-CaO_2-HA for 4 h. Scale bar: 50 μm.

the CD44 receptor, which is highly expressed on tumor cell membranes. After PDT treatment *in vitro*, the survival rates of the 4T1, MCF-7 and LO2 cells were 14.58%, 22.45% and 74.09%, respectively (Fig. 3c). Thus, the cytotoxicity of PCN-224-CaO_2-HA against both 4T1 and MCF-7 cells was much stronger than against normal cells LO2. To verify the targeting effect of HA to tumor cells, the cellular uptake of PCN-224-CaO_2-HA was measured by monitoring the TCPP fluorescence. 4T1, MCF-7 and LO2 cells were incubated with PCN-224-CaO_2-HA, and then imaged using a confocal laser scanning microscope (CLSM). As shown in Fig. 3d, 4T1 and MCF-7 cells presented clear red fluorescence of TCPP, while red fluorescence in LO2 cells was negligible. The results indicated that PCN-224-CaO_2-HA targets 4T1 and MCF-7 cells and presents excellent phototoxicity.

To confirm the above results, a double-staining assay of calcein-AM and propidium iodide (PI) was also used for visual verification of the killing efficiency of the cells *in vitro*, where green and red fluorescence represent living and dead cells, respectively. As shown in Fig. 4a, b and S11,† partial death occurred in both cancer and normal cells treated with PCN-224, demonstrating the excellent PDT performance of the porphyrin-based MOF. In comparison, the PDT effect of PCN-224-CaO_2-HA was superior to that of PCN-224, which might be ascribed to the *in situ* O_2 production of CaO_2 and the targeted effect of HA. Moreover, the apoptosis rate of the 4T1 and MCF-7 cells was higher than that of LO2 cells when treated with PCN-224-CaO_2-HA, which further emphasized the important role of HA in targeted therapy. Besides this, CLSM was used to further study the ROS production in cells after treatment with PCN-224-CaO_2/HA under LED irradiation. 2′,7′-Dichlorofluorescein diacetate (DCFH-DA) is sensitive to the presence of ROS, thus it can be

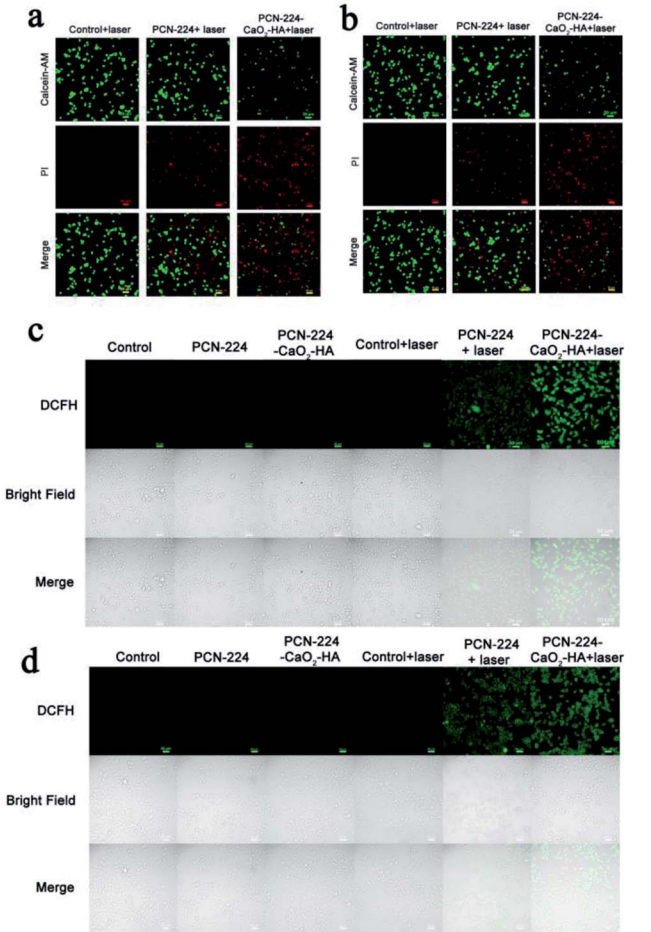

Fig. 4 CLSM images of (a) 4T1 and (b) MCF-7 cells after incubation with PCN-224 or PCN-224-CaO_2-HA under LED irradiation for 10 min (the green color represents live cells and the red represents dead cells). CLSM images of ROS generation in (c) 4T1 and (d) MCF-7 cells incubated with PCN-224 or PCN-224-CaO_2-HA under LED irradiation for 10 min. Scale bar: 50 μm.

used to evaluate the existence of ROS in cells by fluorescence microscopy. As shown in Fig. 4c, d and S12,† the cells treated with PCN-224 or PCN-224-CaO_2-HA in the absence of LED irradiation exhibited negligible fluorescence. Compared with LO2 cells, 4T1 and MCF-7 tumor cells showed strong fluorescence when treated with PCN-224-CaO_2-HA under LED irradiation, which is also consistent with the results of cell survival experiments.

Motivated by the excellent therapy performance *in vitro*, we further investigated the therapeutic efficacy of PCN-224-CaO_2-HA using mice bearing subcutaneous 4T1 tumors. The mice were divided into six groups: (1) control; (2) PCN-224; (3) PCN-224-CaO_2-HA; (4) control + laser; (5) PCN-224 + laser; (6) PCN-224-CaO_2-HA + laser. The tumor sizes in the six groups were monitored every two days in the following 14 days to determine the antitumor effect of the different treatments, as shown in the data in Fig. 5a. In PCN-224 + laser group, the tumor volume was only partially reduced. Notably, remarkable inhibition of tumor growth in the PCN-224-CaO_2-HA + laser group was observed.

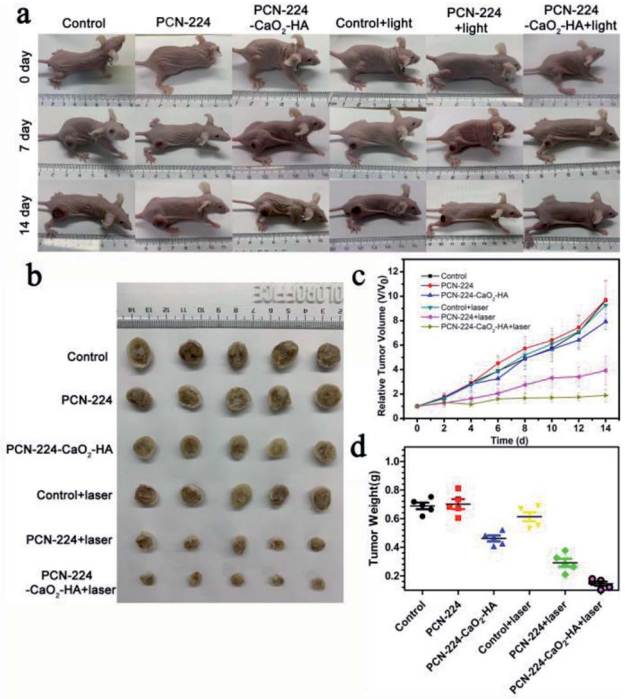

Fig. 5 PDT of mice treated with PCN-224 and PCN-224-CaO_2-HA in a subcutaneous tumor model. (a) Photographs of the 4T1 tumor-bearing mice before treatment and on days 7 and 14 after various treatments. (b) Representative photographs of the tumor dissection. (c) Relative tumor volume after various treatments. (d) Tumor weight after various treatments.

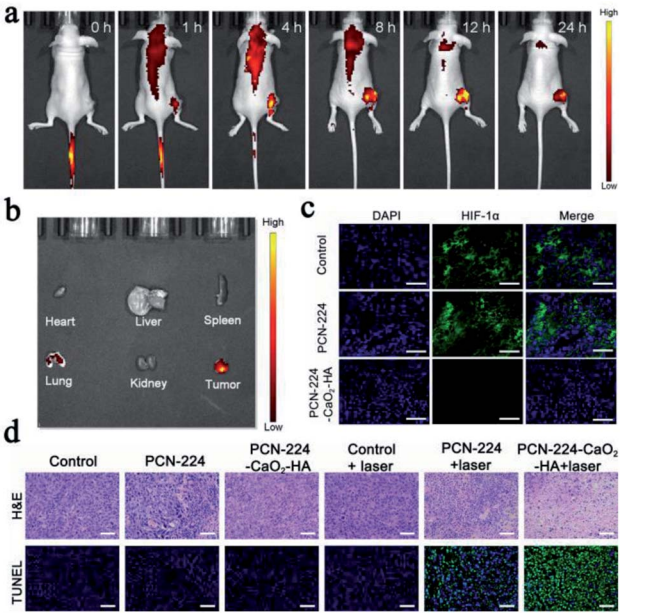

Fig. 6 (a) Fluorescence imaging of 4T1 tumor-bearing mice taken at different time points after intravenous injection with PCN-224-CaO_2-HA. (b) Fluorescence imaging of major organs and tumor after intravenous injection at 24 h. (c) HIF-1α staining tumor tissues harvested from 4T1 tumor-bearing mice treated with PBS, PCN-224 and PCN-224-CaO_2-HA. Green, HIF-1α. Blue, DAPI. (d) H & E and TUNEL staining of tumors subjected to different treatments. Scale bar: 50 μm.

The enhanced therapeutic effect might be ascribed to the specific targeting effect of tumor cells and self-generation of O_2 of CaO_2 (Fig. 5b–d). In addition, PCN-224 and PCN-224-CaO_2-HA showed no significant therapeutic effect without LED irradiation. The body weight was continuously monitored in all mice throughout the entire treatment and the results revealed no changes among the groups, shown in Fig. S13.† This result was also in good agreement with the data *in vitro*.

PCN-224-CaO_2-HA was found to accumulate effectively at the tumor site after 12 h of intravenous administration, which was attributed to the enhanced permeability and retention effect[44] and HA-mediated targeted accumulation of the therapeutic agent (Fig. 6a and b). As expected, obvious fluorescence was recorded at the tumor site, while only a negligible signal was observed in other organs (including heart, liver, spleen, lung and kidney). After 24 h, the fluorescence intensity gradually decreased as a result of the disintegration of PCN-224-CaO_2-HA and the gradual removal of the released TCPP. The mice were sacrificed 24 h later, and the tumor and organs were taken for fluorescence imaging. As shown in Fig. 6b, significant fluorescent aggregation was still observed in the collected tumors, indicating that PCN-224-CaO_2-HA exhibits good retention ability.

After the terminal of therapeutic experiments, the collected tumors were sliced for histological analysis. The expression of the hypoxia inducible factor (HIF-1α) protein as an indicator of tumor hypoxia was also evaluated to further explore hypoxia in the tumor tissues with different treatments (Fig. 6c). The groups treated with PBS and PCN-224 displayed significant green fluorescence, which suggested that HIF-1α was overexpressed. However, the group treated with PCN-224-CaO_2-HA only exhibited slight green fluorescence, which indicated that PCN-224-CaO_2-HA served as an oxygen generator to overcome hypoxia in tumor tissues. The microscopy images of tumor sections for hematoxylin and eosin (H & E) staining and transferase-mediated deoxyuridine triphosphate nick end labeling (TUNEL) are presented in Fig. 6d. H & E staining showed significant tumor cell necrosis and tumor tissue damage in the PCN-224-CaO_2-HA + laser treated group compared with others. Correspondingly, TUNEL staining assay also revealed a higher level of apoptosis. In addition, the main organs of the mice after treatment were dissected and analyzed by H & E staining, which exhibited no evident tissue damage, as shown in Fig. S14.† These results demonstrate that PCN-224-CaO_2-HA exhibits a strong photodynamic effect and good biocompatibility *in vivo*.

Experimental

Materials

Zirconyl chloride octahydrate ($ZrOCl_2 \cdot 8H_2O$) and 5,10,15,20-tetrakis(4-carboxyphenyl)porphyrin (H_2TCPP) were purchased from Jinan Camolai Trading Company. Calcium chloride was purchased from J&K Scientific. Benzoic acid (BA) and sodium hyaluronate were purchased from Shanghai Aladdin Biochemical Technology Co., Ltd. Absolute ethyl alcohol (C_2H_5OH), *N*,*N*′-

dimethylformamide (DMF) and hydrogen peroxide (H_2O_2, 30 wt%) were purchased from Sinopharm Chemical Reagent Co., Ltd. Phosphate buffer (PBS, pH = 7.4), Cell Counting Kit-8 (CCK-8), Calcein-AM/PI, and 2′,7′-dichlorofluorescin diacetate (DCFH-DA) were purchased from Sangon Biotech Co., Ltd. (Shanghai China). Dulbecco's modified Eagle's medium (DMEM) and penicillin–streptomycin solution were purchased from HyClone (Logan City, USA). Fetal bovine serum (FBS) was purchased from PAN-biotech (Aidenbach, Germany). The mouse breast cancer cell line 4T1, human breast cancer cell line MCF-7 and normal human hepatocytes cell line LO2 were purchased from Silver Amethyst Biotech. Co. Ltd (Beijing, China). Ultrapure water was used throughout all of the experiments. The chemicals were of analytical grade and used without further purification.

Instrumentation

Transmission electron microscope (TEM) images were obtained using an H-800 microscope (Hitachi, Japan). Zeta potentials were measured on a Malvern Zetasizer Nano-ZS. PXRD experiments were recorded on a D/Max-2500 X-ray diffractometer using Cu-Kα radiation (λ = 1.5418 Å). X-ray photoelectron spectra (XPS) were recorded using a Thermo Fisher Scientific ESCALAB 250Xi spectrometer (USA). The Ca^{2+} and Zr^{4+} ion contents were measured by inductively coupled plasma mass spectrometry (ICP-MS, 8900, Agilent, USA). The UV-vis spectra were recorded on a Cary 60 UV-vis spectrophotometer (Agilent technologies). The fluorescence measurements were recorded on an F-4600 (Hitachi, Japan) instrument. CCK-8 assay was performed on a microplate reader (DG5033A, China). Confocal fluorescence imaging was performed using a Leica TCS SP8 inverted confocal microscope (Leica, Germany). The cell images were acquired using a 20× objective. *In vivo* imaging was performed using an IVIS Lumina LT imaging system.

Synthesis of PCN-224

150 mg of $ZrOCl_2 \cdot 8H_2O$, 50 mg of H_2TCPP and 1400 mg of benzoic acid were dispersed in 50 mL of DMF in a three-necked flask. Then, the mixture solution was kept in an oil bath at 90 °C for 5 h. At the end of the reaction, the dark purple solid product was collected by centrifugation, followed by washing with fresh DMF three times. Finally, PCN-224 was dried under vacuum at 60 °C.

Synthesis of PCN-224-CaO_2-HA

Firstly, 30 mg of the as-prepared PCN-224 was fully dispersed in 15 mL of absolute methanol. Then, 1 mL of an aqueous solution of sodium hyaluronate (0.5 mg mL^{-1}) and 250 μL of an aqueous solution of calcium chloride (2 mol L^{-1}) were added to the above solution under vigorous stirring. After ten minutes, 700 μL of 30% H_2O_2 was slowly added to this solution at a rate of 1 drop per 10 seconds under constant stirring. After that, ammonia solution was added to the above mixture solution to activate the reaction until a suspended solid was formed. Subsequently, the product was collected by centrifugation, followed by washing it twice with methanol. Thus, PCN-224-CaO_2-HA nanoparticles were obtained.

Detection of ROS

DCFH converted from non-fluorescent DCFH-DA can react with ROS to produce DCF with green fluorescence, which was employed as a probe for ROS measurements. Firstly, 0.5 mL of 1.03 mM DCFH-DA in DMSO was added to 2.0 mL of 0.01 M sodium hydroxide and reacted in the dark at room temperature for 30 min to hydrolyze DCFH-DA to DCFH. Then, the reaction was stopped with 10 mL of sodium phosphate buffer (pH 7.4). Before use, the DCFH solution was kept on ice away from light. In brief, 1 mL aqueous solutions of PCN-224 and PCN-224-CaO_2-HA (30 μg mL^{-1} TCPP) containing the stock solution of DCFH (10 μM) were irradiated using a light-emitting diode (LED, 650 nm). The solution was centrifuged immediately after each irradiation for 1 min, and the fluorescence of the supernatant was measured to estimate ROS.

Dissolved O_2 measurements

15 mg of PCN-224-CaO_2-HA were dispersed in 15 mL of deionized water and the oxygen concentration was monitored per minute using a portable dissolved oxygen meter. As a control, the oxygen concentration of 15 mL of deionized water containing 15 mg of PCN-224 was monitored under the same conditions.

Quantitative analysis of the degradation rate of PCN-224 and PCN-224-CaO_2-HA

Firstly, TCPP standard solutions with concentrations of 0.1, 0.5, 1, 2, 5 and 10 μM were prepared. The absorbance of these solutions at 418 nm was recorded and a standard curve of absorbance and corresponding concentration was plotted. Secondly, PCN-224 and PCN-224-CaO_2-HA were digested by 1 M NaOH for 24 h to fully release TCPP, and the content of TCPP was analyzed using UV-vis spectroscopy. Finally, PCN-224 and PCN-224-CaO_2-HA with the same concentration of TCPP were dispersed in 5 mM PBS buffer, 10 mM PBS buffer and bovine serum, respectively. After 2, 6, 12, 24 and 36 h of incubation, the supernatant was collected and the absorbance at 418 nm was utilized to determine the concentration of TCPP. Thus, the degradation rates of PCN-224 and PCN-224-CaO_2-HA in different solutions were calculated.

Cell culture

4T1, MCF-7 and LO2 cells were cultured in high glucose DMEM supplemented with 10% fetal bovine serum (FBS) and 1% penicillin/streptomycin (P/S), followed by incubation in a standard humidified incubator at 37 °C under an atmosphere containing 5% CO_2. The cells were rinsed once with PBS and then digested with 1 mL of lysis buffer (0.25% trypsin). Then, the cells were collected by centrifugation (800 rpm, 3 min), and plated on 96-well plates or a CLSM-exclusive culture disk one day before the cell viability measurements and cell imaging.

The cell density was determined using a TC20 automated cell counter (Bio-Rad).

Cellular uptake

To study the active targeting ability of PCN-224-CaO_2-HA, 4T1, MCF-7 and LO2 cells were seeded into confocal dishes at a density 1×10^5 cells per well, and the plates were maintained at 37 °C in 5% CO_2 air incubator overnight. Then, the culture medium was replaced with fresh medium containing PCN-224-CaO_2-HA (20 μg mL^{-1} TCPP) and the cells were cultured at 37 °C in 5% CO_2 for 4 h. The cells were washed with PBS three times before imaging was carried out by CLSM.

Cell compatibility

4T1, MCF-7 and LO2 cells were carefully seeded in a 96-well plate (10^4 cells per well) and allowed to adhere overnight. Next, the cells were treated with different concentrations (0, 5, 10, 15, 20, 25 μg mL^{-1} TCPP) of PCN-224-CaO_2-HA for 24 h. The cell viability was measured by CCK-8 assay. Cell viability was evaluated according to the equation: cell viability (%) = $(A_{test} - A_0/A_{control} - A_0) \times 100\%$. A_{test}, A_0 and $A_{control}$ represent the absorbance of experimental group, blank group and control group, respectively.

Cell cytotoxicity

4T1, MCF-7 and LO2 cells were seeded in a 96-well plate (10^4 cells per well) and allowed to adhere overnight. Next, the culture medium was replaced with fresh medium containing PCN-224 or PCN-224-CaO_2-HA at TCPP concentrations of 0, 1.25, 2.5, 5, 10 and 20 μg mL^{-1}. After 4 h, the cells were irradiated under 650 nm LED irradiation for 10 min. After further incubation for 24 h, the old medium was replaced with 10 μL of CCK-8 solution and the cells were cultured. The cell viability was determined by CCK-8 assay.

Intracellular ROS detection

The generation of intracellular ROS was investigated using DCFH-DA as an indicator. In brief, 4T1, MCF-7 and LO2 cells were seeded into confocal dishes at a density 1×10^5 cells and permitted to adhere overnight. Then, the culture medium was replaced with fresh medium containing PCN-224 or PCN-224-CaO_2-HA (20 μg mL^{-1} TCPP) and the cells were incubated for a further 4 h. The dishes were washed with PBS twice and stained with DCFH-DA (10 mM) for 20 min. After that, the cells were washed with 1 × PBS (0.01 M) three times to fully remove DCFH-DA that did not enter the cells and were then irradiated with 650 nm LED irradiation for 10 min. Finally, intracellular ROS generation was observed by CLSM (E_x = 488 nm, E_m = 525 nm).

Live and dead cell assay

4T1, MCF-7, and LO2 cells were seeded in a 6-well plate (10^5 cells per well) for 12 h, followed by incubation with (1) control; (2) PCN-224; (3) PCN-224-CaO_2-HA; (4) control + laser; (5) PCN-224 + laser; and (6) PCN-224-CaO_2-HA + laser, respectively, followed by a further 18 h of incubation. The cells were digested with trypsin and a cell suspension prepared, followed by washing it with PBS buffer three times. The above treated cells were incubated with the calcium AM/PI for 20 min. Next, the cells were transferred to a confocal dish and CLSM was used to obtain the fluorescence images of the stained cells.

Tumor models

All animal studies were conducted in accordance with the Guide for the Care and Use of Laboratory Animals (Ministry of Science and Technology of China, 2006) and approved by the Institutional Animal Care and Use Committee of Linyi University. 4–5 week old female Balb/c nude mice were purchased from Beijing Charles River Laboratory Animal Technology Co., Ltd (China). A tumor model was established by subcutaneously injecting 4T1 cells (1×10^6 cells in 100 μL of PBS) into the right leg of mice.

Antitumor assay *in vivo*

When the tumor volumes reached approximately 100 mm^3, tumor bearing mice were randomly divided into six groups (five mice per group) of (1) control; (2) PCN-224; (3) PCN-224-CaO_2-HA; (4) control + laser; (5) PCN-224 + laser; (6) PCN-224-CaO_2-HA + laser. Then, mice were intravenously treated with PCN-224 or PCN-224-CaO_2-HA (100 μL, 5 mg kg^{-1} TCPP) every 3 days. The control + laser, PCN-224 + laser and PCN-224-CaO_2-HA + laser groups were subjected to 650 nm LED irradiation for 10 min at 12 h after the intravenous injection. The tumor volumes and body weights were measured every two days to evaluate the therapeutic effects. The tumor volume (V) was calculated according to the following equation: $V = L \times W^2/2$. L and W represent the length and width of the tumor, respectively. And the relative tumor volumes of different treated groups were deduced from V/V_0. (in which V_0 is the tumor volume at the beginning of treatment). At the end of the treatment, the mice were sacrificed, and the tumors and major organs (including heart, liver, spleen, lung and kidney) were harvested and fixed in paraformaldehyde (4%), dehydrated, embedded in paraffin, sectioned and stained with H & E (hematoxylin and eosin staining assay). To further study the apoptosis of the tumor cells, the tumor tissues were also subjected to terminal deoxynucleotidyl transferase-mediated dUTP-biotin nick end labeling (TUNEL) staining assays.

Hypoxia study *in vivo*

4T1 tumor-bearing mice were randomly divided into three groups, and then the mice received an intravenous injection of 100 μL of saline, PCN-224 and PCN-224-CaO_2-HA (5 mg kg^{-1} TCPP). 24 h post-injection, all of the mice were sacrificed and the tumor tissues were extracted and HIF-1α staining was performed.

Conclusions

In summary, a self-supplying O_2 nanosystem (PCN-224-CaO_2-HA) based on a MOF combined with hyaluronate-modified CaO_2 nanoparticles was constructed. This nanosystem was able to slowly produce oxygen to reduce hypoxia in the tumor microenvironment, and enhance the effects of PDT.

Hyaluronate protected CaO_2 and specifically targeted the CD44 receptor to perform targeted therapy. The successful *in vitro* and *in vivo* results obtained in this work indicated that PCN-224-CaO_2-HA was able to provide a significantly enhanced therapeutic effect. These facile O_2 self-supplemented and hyaluronate-modified peroxide nanoparticles combined with a MOF might provide perspectives on how to overcome hypoxia in tumors and develop MOF-based targeted therapy.

Author contributions

The authors declare no competing financial interests.

Conflicts of interest

There are no conflicts to declare.

Acknowledgements

This work was supported by the Natural Science Foundation of China (Grant No. 21775062, 21775063 and 22076073) and the China Postdoctoral Science Foundation (No. 2018M642606).

Notes and references

1 S. Fan, Y. Zhang, H. Tan, C. Xue, Y. He, X. Wei, Y. Zha, J. Niu, Y. Liu, Y. Cheng and D. Cui, *Nanoscale*, 2021, **13**, 5383–5399.
2 W. L. Liu, T. Liu, M. Z. Zou, W. Y. Yu, C. X. Li, Z. Y. He, M. K. Zhang, M. D. Liu, Z. H. Li, J. Feng and X. Z. Zhang, *Adv. Mater.*, 2018, **30**, e1802006.
3 A. P. Castano, P. Mroz and M. R. Hamblin, *Nat. Rev. Cancer*, 2006, **6**, 535–545.
4 P. Agostinis, K. Berg, K. A. Cengel, T. H. Foster, A. W. Girotti, S. O. Gollnick, S. M. Hahn, M. R. Hamblin, A. Juzeniene, D. Kessel, M. Korbelik, J. Moan, P. Mroz, D. Nowis, J. Piette, B. C. Wilson and J. Golab, *Ca-Cancer J. Clin.*, 2011, **61**, 250–281.
5 S. Im, J. Lee, D. Park, A. Park, Y. M. Kim and W. J. Kim, *ACS Nano*, 2019, **13**, 476–488.
6 M. Li, J. Xia, R. Tian, J. Wang, J. Fan, J. Du, S. Long, X. Song, J. W. Foley and X. Peng, *J. Am. Chem. Soc.*, 2018, **140**, 14851–14859.
7 K. Han, S. B. Wang, Q. Lei, J. Y. Zhu and X. Z. Zhang, *ACS Nano*, 2015, **9**, 10268–10277.
8 A. Master, M. Livingston and A. Sen Gupta, *J. Controlled Release*, 2013, **168**, 88–102.
9 P. van Driel, M. C. Boonstra, M. D. Slooter, R. Heukers, M. A. Stammes, T. J. A. Snoeks, H. S. de Bruijn, P. J. van Diest, A. L. Vahrmeijer, P. M. P. van Bergen En Henegouwen, C. J. H. van de Velde, C. Lowik, D. J. Robinson and S. Oliveira, *J. Controlled Release*, 2016, **229**, 93–105.
10 D. W. Felsher, *Nat. Rev. Cancer*, 2003, **3**, 375–380.
11 H. Min, J. Wang, Y. Qi, Y. Zhang, X. Han, Y. Xu, J. Xu, Y. Li, L. Chen, K. Cheng, G. Liu, N. Yang, Y. Li and G. Nie, *Adv. Mater.*, 2019, **31**, e1808200.
12 W. Sun, L. Luo, Y. Feng, Y. Cai, Y. Zhuang, R. J. Xie, X. Chen and H. Chen, *Angew. Chem., Int. Ed.*, 2020, **59**, 9914–9921.
13 S. Zhong, C. Chen, G. Yang, Y. Zhu, H. Cao, B. Xu, Y. Luo, Y. Gao and W. Zhang, *ACS Appl. Mater. Interfaces*, 2019, **11**, 33697–33705.
14 G. Wei, L. Huang, Y. Shen, Z. Huang, X. Xu and C. Zhao, *Adv. Ther.*, 2019, **2**, 1900059.
15 Y. Shao, B. Liu, Z. Di, G. Zhang, L. D. Sun, L. Li and C. H. Yan, *J. Am. Chem. Soc.*, 2020, **142**, 3939–3946.
16 S. Gao, Y. Jin, K. Ge, Z. Li, H. Liu, X. Dai, Y. Zhang, S. Chen, X. Liang and J. Zhang, *Adv. Sci.*, 2019, **6**, 1902137.
17 A. B. Ormond and H. S. Freeman, *Materials*, 2013, **6**, 817–840.
18 R. Bonnett, *Chem. Soc. Rev.*, 1995, **24**, 19–33.
19 C. K. Lim, J. Heo, S. Shin, K. Jeong, Y. H. Seo, W. D. Jang, C. R. Park, S. Y. Park, S. Kim and I. C. Kwon, *Cancer Lett.*, 2013, **334**, 176–187.
20 K. Lu, C. He and W. Lin, *J. Am. Chem. Soc.*, 2014, **136**, 16712–16715.
21 G. Lan, K. Ni and W. Lin, *Coord. Chem. Rev.*, 2019, **379**, 65–81.
22 X. Wan, H. Zhong, W. Pan, Y. Li, Y. Chen, N. Li and B. Tang, *Angew. Chem., Int. Ed.*, 2019, **58**, 14134–14139.
23 D. Wang, H. Wu, W. Q. Lim, S. Z. F. Phua, P. Xu, Q. Chen, Z. Guo and Y. Zhao, *Adv. Mater.*, 2019, **31**, 1901893.
24 S. Y. Yin, G. Song, Y. Yang, Y. Zhao, P. Wang, L. M. Zhu, X. Yin and X. B. Zhang, *Adv. Funct. Mater.*, 2019, **29**, 1901417.
25 Y. Zhang, F. Wang, C. Liu, Z. Wang, L. Kang, Y. Huang, K. Dong, J. Ren and X. Qu, *ACS Nano*, 2018, **12**, 651–661.
26 S. Y. Li, H. Cheng, B. R. Xie, W. X. Qiu, J. Y. Zeng, C. X. Li, S. S. Wan, L. Zhang, W. L. Liu and X. Z. Zhang, *ACS Nano*, 2017, **11**, 7006–7018.
27 L. H. Liu, Y. H. Zhang, W. X. Qiu, L. Zhang, F. Gao, B. Li, L. Xu, J. X. Fan, Z. H. Li and X. Z. Zhang, *Small*, 2017, **13**, 1701621.
28 J. H. Yan, W. Meng, H. Shan, X. P. Zhang, L. M. Zou, L. L. Wang, J. S. Shi and X. Y. Kong, *ACS Appl. Nano Mater.*, 2021, **4**, 1351–1363.
29 Y. Han, J. Ouyang, Y. Li, F. Wang and J. H. Jiang, *ACS Appl. Mater. Interfaces*, 2020, **12**, 288–297.
30 M. Zhang, R. X. Song, Y. Y. Liu, Z. G. Yi, X. F. Meng, J. W. Zhang, Z. M. Tang, Z. W. Yao, Y. Liu, X. G. Liu and W. B. Bu, *Chem*, 2019, **5**, 2171–2182.
31 C. Liu, Y. Cao, Y. Cheng, D. Wang, T. Xu, L. Su, X. Zhang and H. Dong, *Nat. Commun.*, 2020, **11**, 1735.
32 Q. Yu, T. Huang, C. Liu, M. Zhao, M. Xie, G. Li, S. Liu, W. Huang and Q. Zhao, *Chem. Sci.*, 2019, **10**, 9091–9098.
33 H. Cheng, P. Yuan, G. Fan, L. Zhao, R. Zheng, B. Yang, X. Qiu, X. Yu, S. Li and X. Zhang, *Appl. Mater. Today*, 2019, **16**, 120–131.
34 Y. Wang, K. Wang, J. Zhao, X. Liu, J. Bu, X. Yan and R. Huang, *J. Am. Chem. Soc.*, 2013, **135**, 4799–4804.
35 E. Blanco, H. Shen and M. Ferrari, *Nat. Biotechnol.*, 2015, **33**, 941–951.
36 K. Zeng, Q. Xu, J. Ouyang, Y. Han, J. Sheng, M. Wen, W. Chen and Y. N. Liu, *ACS Appl. Mater. Interfaces*, 2019, **11**, 6840–6849.

37 S. B. Wang, C. Zhang, X. H. Liu, Z. X. Chen, S. Y. Peng, Z. L. Zhong and X. Z. Zhang, *Adv. Ther.*, 2019, **2**, 1900012.
38 A. Olejek, I. Gabriel, A. Bilska-Janosik, I. Kozak-Darmas and A. Kawczyk-Krupka, *Photodiagn. Photodyn. Ther.*, 2017, **18**, 128–132.
39 Y.-A. Shieh, S.-J. Yang, M.-F. Wei and M.-J. Shieh, *ACS Nano*, 2010, **4**, 1433–1442.
40 B. Yameen, W. I. Choi, C. Vilos, A. Swami, J. Shi and O. C. Farokhzad, *J. Controlled Release*, 2014, **190**, 485–499.
41 Y. C. Zhang, Q. L. Wang, G. Chen and P. F. Shi, *Inorg. Chem.*, 2019, **58**, 6593–6596.
42 K. Kim, S. Lee, E. Jin, L. Palanikumar, J. H. Lee, J. C. Kim, J. S. Nam, B. Jana, T. Kwon, S. K. Kwak, W. Choe and J. Ryu, *ACS Appl. Mater. Interfaces*, 2019, **11**, 27512–27520.
43 Z. Zhou, J. Zhao, Z. Di, B. Liu, Z. Li, X. Wu and L. Li, *Nanoscale*, 2021, **13**, 131–137.
44 H. Maeda, *Cancer Sci.*, 2013, **104**, 779–789.